Ikeda-like chaos on a dynamically filtered supercontinuum light source

Yanne K. Chembo, Maxime Jacquot, John M. Dudley, and Laurent Larger*
FEMTO-ST Institute (CNRS UMR 6174), University Bourgogne Franche-Comté, 15B Avenue des Montboucons, 25030 Besançon cedex, France
(Received 4 June 2016; published 26 August 2016)

We demonstrate temporal chaos in a color-selection mechanism from the visible spectrum of a supercontinuum light source. The color-selection mechanism is governed by an acousto-optoelectronic nonlinear delayed-feedback scheme modeled by an Ikeda-like equation. Initially motivated by the design of a broad audience live demonstrator in the framework of the International Year of Light 2015, the setup also provides a different experimental tool to investigate the dynamical complexity of delayed-feedback dynamics. Deterministic hyperchaos is analyzed here from the experimental time series. A projection method identifies the delay parameter, for which the chaotic strange attractor originally evolving in an infinite-dimensional phase space can be revealed in a two-dimensional subspace.

DOI: 10.1103/PhysRevA.94.023847

Since the pioneering work of Lorenz [1] who demonstrated the phenomenon of sensitivity to initial conditions as predicted by Poincaré [2], chaos theory has been the focus of numerous experimental investigations in order to demonstrate its ubiquity in the real world. It was indeed rapidly identified in many areas, such as chemistry (Belousov-Zabotinski), electronics (Chua's circuit), fluid mechanics (turbulence), solid mechanics (driven pendulum), life sciences, and optics.

In this latter field, a prototype nonlinear optical system of interest was proposed by Ikeda more than 30 years ago [3,4]. His system consisted of a ring optical cavity with a Kerr medium, which was seeded by a continuous-wave (CW) single-mode laser beam. Depending on the input laser intensity level, the phase shift determined by the interference condition at the Kerr medium input can potentially destabilize the optical phase of the intracavity light beam, thus leading to a nontrivial phase dynamics. A simplified model ruling the dynamics of the Ikeda ring cavity results in a scalar first-order delay differential equation of the form

$$\tau \frac{dx}{dt}(t) = -x(t) + \beta \, \sin^2[x(t-\tau_D) + \Phi_0], \qquad (1)$$

where x is the Kerr phase shift, τ stands for the ultrafast light-matter interaction of the Kerr effect, τ_D is the time delay imposed by the cavity roundtrip time, β is the gain of the feedback loop, and Φ_0 is a static offset phase accumulated along the ring cavity. The solutions of this equation have been shown to potentially lead to chaotic fluctuations. From a dynamical systems viewpoint, this setup is characterized by a nonlinear multiple time-scale interaction with significantly different scales, since τ is typically several orders of magnitude smaller τ_D. Ikeda's simulations of the scalar delay differential equation successfully led to the observation of a period-doubling route to chaos. Later on, a convenient optoelectronic implementation of the Ikeda dynamics successfully showed the full bifurcation scenario from a stable steady state to chaos through period doubling [5], and soon after, an integrated electro-optic experimental system was proposed as well to explore the nonlinear behavior of Ikeda-like dynamics [6].

In addition to their relevance, Ikeda-like oscillators have found central applications in optical chaos communications [7–9], ultrastable microwave generation [10,11], and, more recently, photonic brain-inspired processors based on the concept of echo state network (also known as liquid state machine or reservoir computing) [12–15].

In the present article, we report a setup which physically implements an Ikeda-like dynamics according to the conceptual idea of wavelength chaos initially reported in [7]. The latter publication, however, involved an electrically tunable semiconductor laser diode acting as a variable-wavelength light source in the infrared range, with a few angstroms tunability around 1.5 μm. In our reported setup, such a wavelength dynamics is transposed into the full 300 nm visible range of a bright-white light source, a supercontinuum (SC), because of the targeted live demonstration for broad audience dissemination of photonic and nonlinear dynamics phenomena. The electrically driven wavelength-selection mechanism is thus provided by an acousto-optic tunable filter, thereby allowing for a chaotic behavior of a visible color. The experimental system is schematically presented in Fig. 1, which shows the autonomous oscillator architecture with a nonlinear delayed acousto-optoelectronic feedback loop. It consists of the following:

(i) A supercontinuum (SC) source providing an intense white light (25 mW in the visible range). The infrared part of the light source, which represents most of the optical power of the supercontinuum, is filtered out since it is not relevant to our primary objectives and could represent an eye danger during the experiment. We used a commercial SC providing an already collimated beam with approximately 1 mm diameter. Principally, a white light emitting diode could be used as well; however, that would require more electronic feedback gain and a dark environment for the observation of the color dynamics.

(ii) An on-axis acousto-optic tunable filter (AOTF), allowing for the fast (a few μs response time) and nearly linear selection of a color (spectral slice of approximately 4 nm width in the blue range until 16 nm in the red range) within the supercontinuum visible spectrum. The input signal ruling the selection is a 0.5 watt radio-frequency waveform, spanning from 74 MHz (selecting the red color) to 158 MHz (blue color). Since the AOTF is polarization sensitive and

*laurent.larger@femto-st.fr

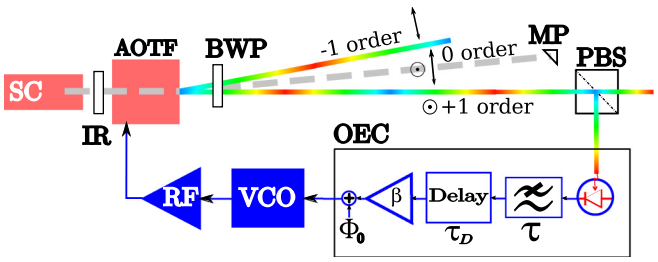

FIG. 1. Schematic representation of the visible-wavelength nonlinear delayed-feedback loop oscillator. SC: collimated supercontinuum light source; IR: infrared blocking filter; AOTF: acousto-optic tunable filter; BWP: birefringent quartz wave plate; PBS: polarization beam splitter; MP: mirror prism extracting the zero-order AOTF output, for further display of rainbows through mirrors and diffraction gratings; OEC: optoelectronic circuit performing photodetection, filtering, delaying, amplification, and offset setting; VCO: voltage-controlled oscillator; RF: radio-frequency driver.

since the supercontinuum does not provide a polarized light beam, one obtains three angularly separated output beams: the $(+1)$ on-axis order, with the proper AOTF polarization state, and corresponding to the selected color; the (-1) off-axis order, containing the same selected color, but with an orthogonal polarization state and with a wavelength-dependent angular deviation; and the zero off-axis order, gathering all the nonselected colors, i.e., an unpolarized white light beam from which the selected color is removed (the AOTF has more than 90% efficiency for the selected color).

(iii) A commercial X-cut quartz birefringent plate, which thickness was reduced down to 250 μm, such that the corresponding optical path difference over the visible range results in a maximum of 2π phase shift. The wave plate is oriented, as usual for a birefringent filter with maximized contrast, at 45° from the polarization state of the selected color.

(iv) A polarization beam splitter oriented parallel or perpendicular to the AOTF output polarization state, and providing two complementary interference states at its two outputs. This device generates at its output the two-wave interference modulation transfer function ($\cos^2$ or $\sin^2$), fulfilling the role of the nonlinear transformation in the dynamical delayed feedback.

(v) A silicon photodiode converts the intensity interference into an electrical amplitude, which can then be processed electronically: The signal is delayed in time by an electronic delay line [analogue first-in first-out (FIFO) memory providing a time delay $\tau_D \simeq 0.5$ s, which can be easily followed by the eye response time, again for a broad audience live demonstrator target]. The electronic signal is also low-pass filtered to force the resulting wavelength change to also occur within the human-eye bandwidth, typically with 3 Hz cutoff frequency ($\tau \simeq 50$ ms response time). Gain and offset can be adjusted through two variable resistors which are defining the constant voltages used in a standard multiplier circuit using an AD633, thus allowing for the tuning of parameters β and Φ_0 in Eq. (1), respectively.

(vi) The output signal of the previous photodetection, delaying, filtering, offsetting, and amplifying functions, serves then as the input of a voltage-controlled oscillator (VCO). This device delivers a constant-amplitude RF output, which RF frequency (in the 74–158 MHz range) is proportional to the input voltage amplitude (between 0 and 10 volts).

(vii) An RF amplifier is finally required before electronically feeding the AOTF, in order to have the 0.5 W RF power needed to operate the AOTF at its maximum diffraction efficiency, above 90%.

Additional technical details need to be considered in order to optimize the matching of the model of this setup with the Ikeda one in Eq. (1). First, one needs to filter the detected optical intensity to average the actual pulsed SC light source. Since the global dynamics is limited by a 3 Hz low-pass cutoff and the SC repetition rate can be set to 20 kHz, a passive first-order RC filter right after the photodiode with a 200 Hz cutoff easily extracts the average intensity of the interfering SC light pulses: Most of the pulse harmonics are thus removed and the electronic image of the intensity is properly smoothed to correspond to a continuous-time dynamics. Another important issue concerns the combined effect of the nonflatness of the SC spectral density, and the nonconstant spectral response of the silicon photodiode. Without any dedicated compensation, the red side of the spectrum appears to have a much higher gain than the blue one. The adopted solution is to passively compensate this through a properly adjusted linear color-dependent gain with a simple multiplier circuit after photodetection. The gain input of the multiplier is thus designed from a proper amplification and offsetting of the voltage driving the VCO (and thus selecting the color, i.e., low voltage for red and high voltage for blue).

For appropriate gain (β) and offset (Φ_0) to be adjusted on the electronic board, a visual demonstration of the Ikeda dynamics complexity can be obtained. One can, of course, monitor the input voltage of the VCO, but more interestingly in this setup, one directly sees from the different AOTF light-beam outputs the nicely color-encoded motion corresponding to the obtained dynamics. There are actually three such possible visualizations: The (-1) AOTF diffraction order, which is unused by the delayed feedback loop, but shows the selected color during the dynamics; the second interferometer output from the polarization beam splitter, which shows the selected color with a complementary interference intensity with respect to the one of concern in the dynamics; and the zero order at the AOTF output which appears as an intense white light beam—but once spatially spanned by a diffraction grating, a bright rainbow is observed in which a moving dark line is clearly seen. This dark line corresponds to the absence of the color actually selected by the AOTF.

The latter visualization (through the zero-order AOTF output) was used in practice in our setup. We have also used white screen projectors to display and monitor the supercontinuum rainbows with the chaotically moving dark line. In order to generate such rainbows, we have exploited the high brightness of the SC light source, and we used 20% diffraction efficiency gratings, from which the complementary 80% zero order was recycled with mirrors, thus allowing us to reuse the remaining nondiffracted light through further gratings with different projection directions and different diffraction orientations. Please see Supplemental Material [16] for a short video of the physical setup in the lab, while operating in a

chaotic regime. The movie shows a moving dark line within a grating-diffracted zero order, the arrangement of the different devices forming the full acousto-electro-optoelectronic setup, as well as a short live time trace of an electronic signal proportional to the normalized dynamical variable $x(t)$.

From the nonlinear dynamics viewpoint, the setup also allows one to understand and monitor the temporal chaotic behavior of the visible-wavelength dynamics. In particular, the fact that all of the time scales are slowed down, such that everything can be directly captured by the human eye (time scale of the order of seconds), allows one to very easily reveal the numerous transients during convergence towards an attractor (a usually neglected phenomenon, but interesting in many aspects, e.g., the local dynamical properties of an attractor, the real or complex nature of the related eigenvalues, etc.). Numerous complex slow-fast dynamical phenomena could also be explored with this setup, as already reported in experiments belonging to the same class of delay dynamical systems [17–22]. We have particularly focused on the exploration of the chaotic regimes. The corresponding time trace in presented in Fig. 2, and the envelope dynamics displays the characteristic pseudorandom oscillations of chaotic Ikeda systems, with a time scale of the order of seconds. The autocorrelation function shown in Fig. 2 features typical peaks at lag times approximately equal to $\pm(\tau + \tau_D)$, as it is known from chaotic Ikeda systems, which feature flat spectra below the low-pass cutoff frequency as well in the chaotic regime (see Fig. 2).

In order to provide unambiguous evidence of the deterministic chaotic nature of the pseudorandom behavior displayed in Fig. 2, we use the filling-factor method for dynamical systems, which is a well-known accurate method that can be used to extract the precise delay value from a time series ruled by a delay differential equation [23,24]. The method was used, for example, in chaos communications cryptanalysis [25], for which the most important parameter to recover first is precisely the time delay. The method is used in this work to unambiguously evidence the deterministic feature in the recorded experimental time traces, and its basic principle is as follows. Despite the fact that the dynamics is infinite

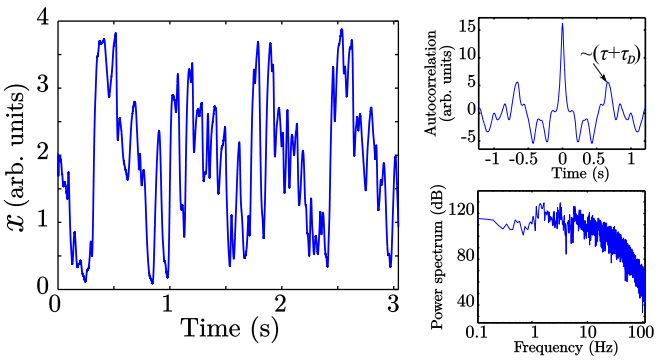

FIG. 2. Part of a chaotic signal. The two right plots are calculated from a long chaotic time series [top: autocorrelation function revealing the echo in the chaotic time series at approximately $(\tau + \tau_D)$; bottom: amplitude of the Fourier spectrum, showing the nearly flat filling of the Fourier components within the oscillator bandwidth].

dimensional, there exists a low-dimensional subspace in which a strong constraint is imposed by the dynamical equation of motion. In the case of a conventional scalar nonlinear delay dynamics (Ikeda, Mackey-Glass, etc.), one simply has to construct a three-dimensional (3D) vector trajectory from a time series, which vector coordinates are $[\dot{x}(t),x(t),x(t-\tau_s)]$, where τ_s is a time shift. When τ_s precisely matches the time delay τ_D of the original equation of motion, the trajectory lies on a surface. Plotting the volume filled by the trajectory in this 3D space as a function of τ_s will reveal a nearly constant value corresponding roughly to a cube of a volume $[\max(x) - \min(x)]^3$, except when $\tau_s = \tau_D$ for which time shift the volume shrinks sharply to zero because one has to have a surface. This technique can be further simplified in a 2D space, plotting the points $[x(t_k), x(t_k - \tau_s)]$, where t_k are the dates of the original time trace exhibiting extrema, i.e., $\dot{x}(t_k) = 0$. The calculation of the surface covered in the 2D plane $[x(t_k), x(t_k - \tau_s)]$ can be approximated, when using a finite number of dates t_k for the extrema of the time trace, as

$$\rho = \frac{1}{L-1} \sum_{l=1}^{L} \frac{\max[x_l(t_k)] - \min[x_l(t_k)]}{\max(x) - \min(x)}, \qquad (2)$$

where the interval in x (that is, $[\min(x), \max(x)]$) visited by the trajectory is divided into $(L-1)$ subintervals of the kind $\Delta_l = [x_l, x_{l+1}]$ for $l = 1$ to L. For each value $x(t_k - \tau_s)$ belonging to one such interval, we collect the values $\{x_l(t_k) = x(t_k) | x(t_k - \tau_s) \in \Delta_l\}$. The definition of ρ involves the amplitude span $\{\max[x_l(t_k)] - \min(x_l[t_k])\}$ in each of these $(L-1)$ sets $\{x_l(t_k)\}$. The filling factor ρ is plotted as a function of the time lag τ_s in Fig. 3. It appears that ρ sharply drops to zero when the lag time matches the delay time, while

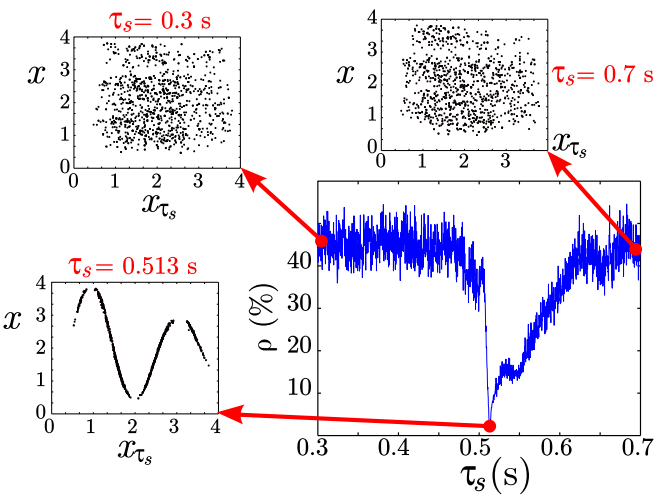

FIG. 3. Plot of the filling factor ρ as a function of the time lag τ_s, following the definition of Eq. (2). Note that the filling factor sharply drops to a value very close to zero when the lag time fulfills the condition $\tau_s = \tau_D = 0.513$ s. In that case, the dynamics of the system is projected onto the nonlinear transfer function in the plane $x_{\tau_s} - x$. On the other hand, when τ_s is significantly different from the time delay τ_D, the dynamics of the system in the plane $x_{\tau_s} - x$ is chaotically distributed. This plot provides evidence about the fact that the dynamics displayed in Fig. 2 is a chaotic behavior resulting from the nonlinear Ikeda feedback loop.

the dynamics is projected onto the quasisinusoidal transfer function in the plane $x_{\tau_s} - x$, thereby providing a proof that the slowly varying envelope of the supercontinuum spectrum displayed in Fig. 2 follows an Ikeda-like chaotic behavior. The Supplemental Material [16] provides a video file of the moving dots in the $x_{\tau_s} - x$, while τ_s is finely incremented from 0.3 s to 0.7 s with with 0.25ms increment every movie frame. The first frame, as well as the last one and the one corresponding to the matching of τ_s with the correct delay value τ_D, are represented in the insets of Fig. 3.

In conclusion, we have reported the Ikeda-like temporal chaotic behavior of a color dynamically sliced in the visible spectrum of a supercontinuum light source. This complex behavior has been analyzed using the various tools of time-series analysis such as the autocorrelation plot, the power Fourier spectrum, and the filling-factor curves. Perspectives for future research are numerous for these chaotic rainbows. This system could include as well a high-pass filtering in the electronic feedback [26], resulting in an integral slow time scale responsible for the occurrence and stabilization of many additional dynamical motions, such as chaotic breathers [27] or single-delay periodic motions [28]. Further scientific issues could also concern the observation of chimera states [29,30] in this visible-wavelength delay dynamics. Such a particular complex and self-organized motion should also be observable in this visible-wavelength dynamics, if some of the system features can be adequately modified. One would need to first implement a slow integral time scale through a high-pass filtering in the feedback loop, and second replace the birefringent filter by a Fabry-Pérot one which exhibits a strong asymmetry between the minima and maxima of the nonlinear transformation. Other investigations could concern a possible smooth-transition scenario between the continuous-time delay differential equation model and its discrete-time singular limit map approximation [31], once the time scales of the dynamics can be controlled such that SC light pulses can be time resolved in the delayed-feedback loop.

The setup can also be used within a teaching perspective in physics, optics, and nonlinear dynamics. Various phenomena can be easily illustrated by direct or indirect visual observation.

Finally, since the experiment was initially motivated by dissemination and broad audience scientific demonstration issues in the framework of the International Year of Light 2015, one might also conclude with a fortuitous and surprising comment linking the history of arts and sciences through the chaotic rainbow setup. Indeed, the famous French painter Cézanne once said, "We live in a rainbow of chaos." It is then surprising to realize that Cézanne was a contemporary of Poincaré, one of the precursors of chaos theory through his seminal work on nonlinear dynamical systems. "Chaos" was, however, proposed much later on in the 1970s, by Li and Yorke [32], as a name for the kind of dynamical system solutions exhibiting sensitivity to initial conditions.

This work was supported by the Region Franche-Comté (CORPS project), the Labex ACTION (Contract No. ANR-11-LABX-01-01), and the IDEFI CMI-FIGURE French higher education program (Contract No. ANR-11-IDFI-0010). The authors thank P. Roux, E. Dordor, L. Gauthier-Manuel, L. Furfaro, R. Giust, J.-M. Merolla, L. Illing, B. Beausire, F. Berther, J. Nguyen, V. Armbruster, J. Nunes, R. Bourquin, J.-C. Savoie, P. Roblot, and L. Tournier for their contribution to the design and implementation of the experimental setup.

[1] E. N. Lorenz, J. Atmos. Sci. **20**, 130 (1963).
[2] H. Poincaré, *Les Méthodes Nouvelles de Mécanique Céleste* (Gauthier-Villars, Paris, 1893).
[3] K. Ikeda, Opt. Commun. **30**, 257 (1979).
[4] K. Ikeda, H. Daido, and O. Akimoto, Phys. Rev. Lett. **45**, 709 (1980).
[5] H. M. Gibbs, F. A. Hopf, D. L. Kaplan, and R. L. Shoemaker, Phys. Rev. Lett. **46**, 474 (1981).
[6] A. Neyer and E. Voges, IEEE J. Quantum Electron. **18** 2009 (1982).
[7] J.-P. Goedgebuer, L. Larger, and H. Porte, Phys. Rev. Lett. **80**, 2249 (1998).
[8] A. Argyris, D. Syvridis, L. Larger, V. Annovazzi-Lodi, P. Colet, I. Fischer, J. Garcia-Ojalvo, C. R. Mirasso, L. Pesquera, and A. K. Shore, Nature (London) **438**, 343 (2005).
[9] R. Lavrov, M. Jacquot, and L. Larger, IEEE J. Quantum Electron. **46**, 1430 (2010).
[10] X. S. Yao and L. Maleki, Electron. Lett. **30**, 1525 (1994).
[11] L. Maleki, Nat. Photon. **5**, 728 (2011).
[12] L. Larger, M. C. Soriano, D. Brunner, L. Appeltant, J. M. Gutierrez, L. Pesquera, C. R. Mirasso, and I. Fischer, Opt. Express **20**, 3241 (2012).
[13] R. Martinenghi, S. Rybalko, M. Jacquot, Y. K. Chembo, and L. Larger, Phys. Rev. Lett. **108**, 244101 (2012).
[14] D. Woods and T. J. Naughton, Nat. Phys. **8**, 257 (2012).
[15] D. Brunner, M. C. Soriano, C. R. Mirasso, and I. Fischer, Nat. Commun. **4**, 1364 (2013).
[16] See Supplemental Material at http://link.aps.org/supplemental/10.1103/PhysRevA.94.023847 for two video illustrations.
[17] A. B. Cohen, B. Ravoori, T. E. Murphy, and R. Roy, Phys. Rev. Lett. **101**, 154102 (2008).
[18] T. Erneux and P. Glorieux, *Laser Dynamics* (Cambridge University Press, Cambridge, 2010).
[19] T. Erneux, *Applied Delay Differential Equations* (Springer, New York, 2010).
[20] K. E. Callan, L. Illing, Z. Gao, D. J. Gauthier, and E. Schöll, Phys. Rev. Lett. **104**, 113901 (2010).
[21] L. Larger and J. M. Dudley, Nature (London) **465**, 41 (2010).
[22] B. Ravoori, A. B. Cohen, J. Sun, A. E. Motter, T. E. Murphy, and R. Roy, Phys. Rev. Lett. **107**, 034102 (2011).
[23] R. Hegger, M. J. Bünner, H. Kantz, and A. Giaquinta, Phys. Rev. Lett. **81**, 558 (1998).
[24] B. P. Bezruchko, A. S. Karavaev, V. I. Ponomarenko, and M. D. Prokhorov, Phys. Rev. E **64**, 056216 (2001).
[25] V. S. Udaltsov, J.-P. Goedgebuer, L. Larger, J.-B. Cuenot, P. Levy, and W. T. Rhodes, Phys. Lett. A **308**, 54 (2003).

[26] L. Larger, Philos. Trans. R. Soc. A **371**, 20120464 (2013).
[27] Y. C. Kouomou, P. Colet, L. Larger, and N. Gastaud, Phys. Rev. Lett. **95**, 203903 (2005).
[28] L. Weicker, T. Erneux, O. DHuys, J. Danckaert, M. Jacquot, Y. Chembo, and L. Larger, Philos. Trans. R. Soc. A **371**, 20120459 (2013).
[29] L. Larger, B. Penkovsky, and Y. Maistrenko, Phys. Rev. Lett. **111**, 054103 (2013).
[30] L. Larger, B. Penkovskyi, and Y. L. Maistrenko, Nat. Commun. (London) **6**, 7752 (2015).
[31] L. Larger, P.-A. Lacourt, S. Poinsot, and M. Hanna, Phys. Rev. Lett. **95**, 043903 (2005).
[32] T.-Y. Li and J. A. Yorke, Am. Math. Monthly **82**, 985 (1975).